TWO-DIMENSIONAL NUMERICAL MODELS FOR THE HIGH ELECTRON MOBILITY TRANSISTOR

Dany Loret(*), Roel Baets(*), Christopher M. Snowden(**), and William J. Hughes(***)

* University of Ghent - IMEC, Laboratory of Electromagnetism and Acoustics (L.E.A), St.-Pietersnieuwstraat 41, 9000 Ghent, Belgium

** Microwave Solid State Group, Department of Electrical and Electronic Engineering, University of Leeds, Leeds, LS2 9JT. England.

*** GEC Hirst Research Centre, East Lane, Wembley, Middlesex, HA9 7PP. England.

ABSTRACT

A two-dimensional drift-diffusion model for the high electron mobility transistor (HEMT) is described. Special attention is paid to the modeling of the AlGaAs/GaAs heterojunction. Also, an energy transport model for the HEMT is proposed. The internal distributions of electron density, voltage and current density are discussed. The influence of hot electron effects in HEMT's is demonstrated. The results obtained using these models are found to agree with those obtained from experimental devices.

1.INTRODUCTION

In the last few years, more and more attention has been paid to the high electron mobility transistor, both from experimental and theoretical point of view. The first HEMT models presented were one-dimensional analytical models, based on quantummechanics [1]-[3]. These models establish a relationship between the total number of electrons in the channel of the transistor, the so-called two-dimensional electron gas, and the gate voltage. By self-consistent integration from source to drain, the external current-voltage characteristics are then determined. The performance of these models is increased with the detailed implementation of device physics, such as parallel conduction in the AlGaAs layer [4].

Two-dimensional numerical simulation models for homojunction MESFET's are well established nowadays [5],[7].

They have been developed in order to describe more accurately a number of phenomena, that could not be analysed with more simple analytical models, especially when device geometry becomes smaller. More recent simulations have included hot electron effects [8]-[10]. These energy transport models are shown to give a better description of submicron device physics. Up to now, reports on two-dimensional models for HEMT's are rather sparse. Yoshida et al. [11] and Tang [12] reported a 2D drift-diffusion model for HEMT's. Widiger et al. [13],[14] developed a 2D energy transport model. A review of AlGaAs/GaAs device modeling has been given by Bennett [15].

The models described in sections 2 and 3 are a 2D drift-diffusion model and a 2D energy transport model for the HEMT. For both models, device geometry has been simulated accurately by placing all three contacts at the surface. In addition, special attention has been paid to the calculation of the current normal to the AlGaAs/GaAs heterojunction. Section 3 includes a short description of the numerical approach. In section 4 modeling results are discussed and compared with some experimental measurements.

2. PHYSICAL DEVICE MODELS

A. 2D Drift-Diffusion Model

The model of the HEMT is based on a two-dimensional geometry of the form shown in figure 1. The actual device geometry is the one shown in figure 2. In the model only three basic layers are considered: a highly doped $Al_xGa_{1-x}As$ toplayer, an undoped $Al_xGa_{1-x}As$ spacer layer and an undoped GaAs buffer layer. All three contacts are placed on top of the AlGaAs layer. A GaAs highly doped cap layer, as used in the practical device, is omitted in the model, as well as deeper buffer layers and the GaAs substrate.

The model is based on Poisson's equation together with the macroscopic transport equations commonly used [6]:

Poisson's equation:

$$\vec{\nabla}.(\varepsilon\varepsilon_0)\vec{\nabla}V = q(n-N_D) \tag{1}$$

Continuity equation:

$$\frac{\partial n}{\partial t} = \frac{1}{q}\vec{\nabla}.\vec{J} \tag{2}$$

Current density equation:

$$\vec{J} = -qn\mu\vec{\nabla}V + kT\mu\vec{\nabla}n \tag{3}$$

In these equations V stands for voltage, $\varepsilon\varepsilon_0$ the dielectric

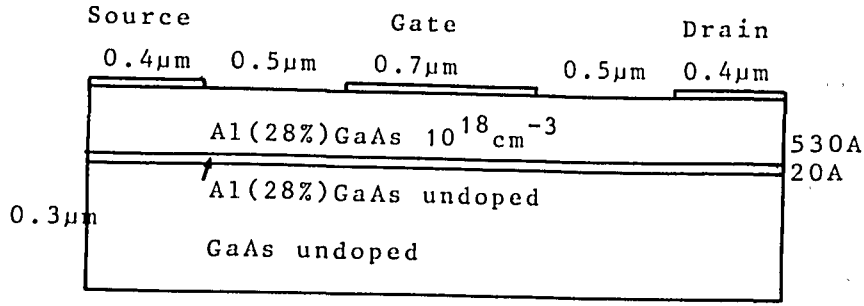

Fig.1 : Device geometry used in the models

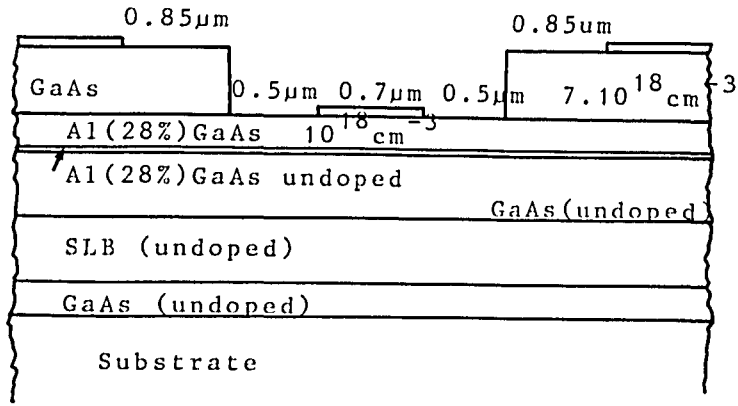

Fig.2 : Experimental device geometry

permittivity of the material, q electronic charge magnitude, n electron density, N_D doping density, t time, $\vec{J}$ current density, µ mobility, k Boltzmann constant and T lattice temperature. All variables are considered to be functions of the two independent position coordinates. Time dependence has been retained, so that both steady-state operation and transients can be simulated. To make allowance for the uncertainty on the field-velocity dependence of GaAs, especially near the heterojunction, simulations have been done with two different curves (figure 3). The mobility in the AlGaAs layer is low, due to the high doping density. The dependency on the Al mole faction of device parameters was taken from [16].

Equation (3) is valid in the whole semiconductor region considered, except for current calculation normal to the abrupt heterojunction. In addition, a thermionic emission expression is used in the form of Schuelke and Lundstrom [17]:

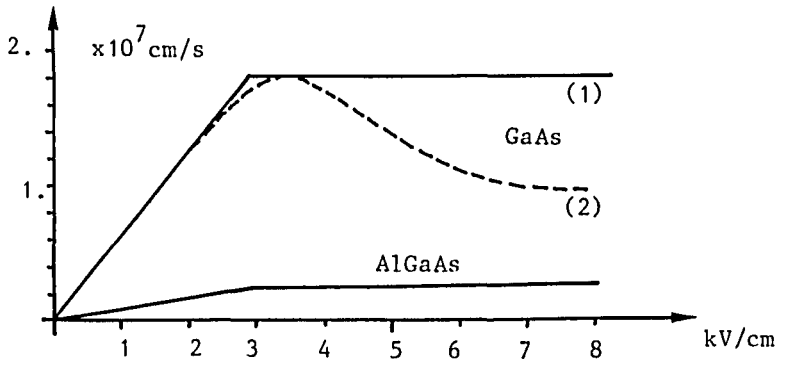

Fig.3 : Drift velocity versus field

$$J_n = -qS_n\left[n(x_j^-) - n(x_j^+)\exp\left(\frac{-\Delta V_n}{kT}\right)\right].\gamma_n \qquad (4)$$

where J_n denotes the current density normal to the heterojunction, S_n the interface velocity, $n(x_j^-)$ and $n(x_j^+)$ the electron density near the junction at the AlGaAs side and at the GaAs side respectively. ΔV_n is the discontinuity in the electron band parameter:

$$\Delta V_n = \Delta\chi + kT\log\left[\frac{N_c(x_j^+)}{N_c(x_j^-)}\right] + kT\log\left[\frac{F_{1/2}(\eta_c)}{\exp(\eta_c)}\right] \qquad (5)$$

where χ stands for electron affinity and N_c for effective density of states. The discontinuity in the conduction band $\Delta\chi$ is taken to be 62% of the band gap discontinuity, after recent experimental data. The third term in the right member denotes a correction term to take Fermi-Dirac statistics into account [17]. Tunneling has been taken into account through the inclusion of a factor γ_n, using an approach found in [18] for a triangular barrier.

Subband splitting in the two-dimensional electron gas, as predicted by models based on quantummechanics, has not been taken into account. It has been shown [11],[19] that the classical approach with Boltzmann statistics predicts a sheet electron concentration which is in the order of 20% higher than the concentration predicted by an exact quantummechanical calculation. The use of Fermi-Dirac statistics reduces this error to within a few percent.

B. 2D Energy Transport model

The device geometry for this model is the same as for the drift-diffusion model. The transport equations (2) and (3) are replaced by four equations in the form of Widiger [14]:

$$\frac{\partial n}{\partial t} = \frac{1}{q}\vec{\nabla}.\vec{J} \tag{6}$$

$$\vec{J} = -qn\mu\vec{\nabla}V + \vec{\nabla}(\mu k T_e n) \tag{7}$$

$$\frac{\partial W}{\partial t} = -\vec{J}.\vec{\nabla}V - \frac{W-W_0}{\tau} - \vec{\nabla}.\vec{S} \tag{8}$$

$$\vec{S} = \mu W\vec{\nabla}V - \frac{1}{q}\vec{\nabla}(\mu k T_e n) \tag{9}$$

In these equations, W stands for the electron energy density, W_0 the equilibrium value, τ energy relaxation constant, and $\vec{S}$ the energy flux. T_e is the electron temperature, related to the electron energy density:

$$T_e = \frac{2qW}{3nk} \tag{10}$$

In this model, mobility μ and relaxation constant τ are functions of the electron temperature. The approach of Snowden [10] has been used.

In addition to the drift and diffusion currents, a contribution to the total current density comes from electron temperature gradients in (7). The energy balance equation (8) states that the energy density changes are due to heating by the electric field, energy loss due to collisions and transport of energy through the system. This transport is described by (9). Only heating due to longitudinal fields is taken into account. Equation (4) still holds to describe the current normal to the junction, if the lattice temperature T is replaced by the electron temperature T_e.

3. NUMERICAL SOLUTION

The time dependent device equations were solved numerically in two dimensions using a finite difference scheme. A variable mesh spacing is used to optimize speed and accuracy of the solution. Space stepwidths vary from 0.08 μm to 0.02 μm in the longitudinal direction, and in the transverse direction from 0.03 μm to 2 nm near the heterojunction (figure 4). Time steps are kept less than 10 fs for the drift-diffusion model, and even less than 1 fs for the energy transport model, in order to preserve numerical stability. Poisson's equation was solved using LU-factorisation. A modified Scharfetter-Gummel algoritm

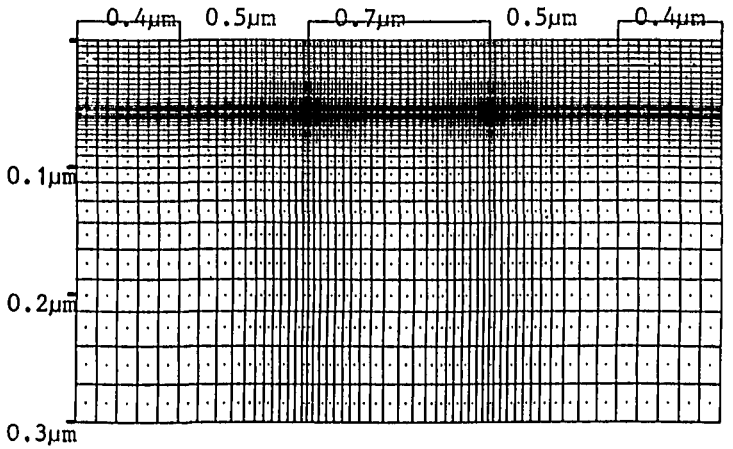

Fig.4 : Finite differences grid

[6],[20] was used to transform the current and energy continuity equations. Both equatios have the same coefficients, but have different right members. With the unknown variables n and W respectively, they are solved with a simple under-relaxation iterative scheme. By integration over the contacts, the external currents can be determined. The models have been developed on a VAX II 750 computer.

4. RESULTS AND DISCUSSION

The results discussed below are based on simulations with the velocity - field curve 1 (figure 3). Additional simulation results with the use of curve 2 will be given in the presentation.

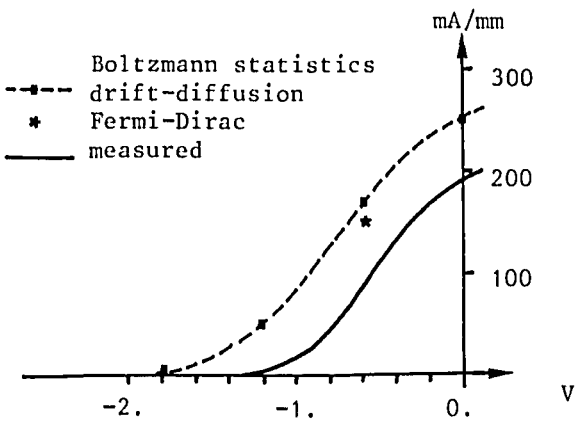

Fig.5 : Calculated and measured I_D versus V_{GS}

Figure 5 shows the I_D versus V_{GS} curve at V_{DS} = 4.V, as a result from drift-diffusion model simulations. These results are compared with the corresponding experimental data. Currents predicted by the model turn out to be too high, which, as seen

from the figure, is due to a threshold voltage being 0.5V more negative in the model. This could be due to the use of Boltzmann statistics in the model. Therefore an additional simulation has been done including Fermi-Dirac statistics, for $V_{GS} = -0.6V$ and $V_{DS} = 4.V$. This simulation resulted in an 8% drain current decrease, which corresponds to the findings of Yoshida [19]. Clearly, there still is a discrepancy between the calculated and measured result. This is most probably due to some uncertainty on the device parameters, especially the velocity - field relationship. The transconductance g_m is defined as the slope of the I_D versus V_{GS} curve:

$$g_m = \frac{\partial I_D}{\partial V_{GS}} \mid V_D = \text{const} \tag{11}$$

There is a good agreement between theoretical and experimental results (figure 6). A maximum value of 200 mS/mm respectively 180 mS/mm has been found in both cases. This maximum occurs at slightly different gate voltages, reflecting again the threshold voltage mismatch. Since both AlGaAs and GaAs layers were taken into account in the simulations, it was possible to determine the total gate capacity C_G, and hence unity gain frequency f_T:

$$C_G = \frac{\partial Q}{\partial V_{GS}} \mid V_D = \text{const} \tag{12}$$

$$Q = \int\int qn dx dy \tag{13}$$

$$f_T = \frac{1}{2\pi} \frac{g_m}{C_G} \tag{14}$$

These quantities are shown in figure 6.

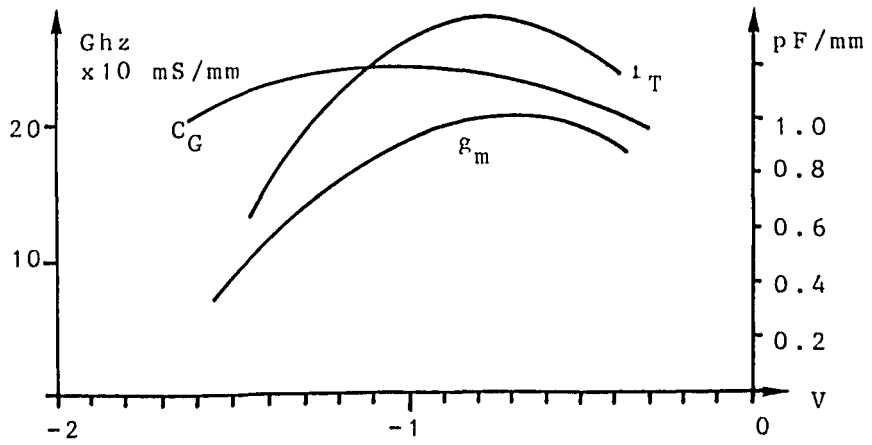

Fig.6 : C_G, g_m and f_T versus gate voltage

The unity gain frequency reaches a maximum value of 28 GHz for V_{GS} = -0.6V. For higher gate voltages a decrease in f_T is caused by a decrease in transconductance. Again a good agreement is found with experimental S_{21} measurements, which showed a unity gain frequency of 25 GHz.

Figure 7 shows the conduction band profile at V_{DS} = 4.V and V_{GS} = 0.V. Most of the voltage drop between source and drain occurs at the drain end side of the channel, smoothed out towards the substrate. Due to the small spacing between source and drain, the longitudinal component of the electric field is higher than the critical field from the v(E) relationship in the whole channel, so that electrons move with saturation velocity. One can observe the conduction band discontinuity at the heterojunction which is 0.22V.

Figures 8 and 9 show the electron density for V_{DS} = 4.V, V_{GS} = 0.V and V_{GS} = -1.8V respectively, representing on and off states of the transistor. In figure 10, this information is presented in contour plot form. Near the heterojunction a depletion layer exists at the AlGaAs side and an accumulation layer at the GaAs side of the junction. In our model all the carriers, including those in the 2-D electron gas, are numerically treated as bulk carriers, obeying Fermi-Dirac statistics. This contrasts with the approach of Widiger [14] where a sheet of carriers is used to describe the 2-D electron gas, interacting with the bulk carriers. It can be seen from our figures that in the source and drain regions more than 90 % of the electrons are in a 20 nm wide accumulation region. In addition, one can see from figure 10 that electrons are injected into the substrate at the drain end side of the channel, as was reported by Yoshida. Widiger has also found that towards the drain end side of the channel current is mainly established by bulk GaAs electrons. However, this effect is rather weak, and most of the current is still flowing immeadiately near the junction. Further towards the drain, the electrons are confined in the well again, and cross the junction to the drain.

An important effect is the presence of electrons in the AlGaAs layer under the gate, occuring at higher gate voltages. This results in parallel conduction in the toplayer. However, at a certain point under the gate, most electrons cross the heterojunction, so that the longitudinal current density at the end of the channel is entirely situated in the GaAs. The presence of electrons in the AlGaAs layer under the gate is the reason for the decrease of transconductance at higher gate voltages. With an increasing carrier density in the AlGaAs, the total concentration of electrons in the channel starts to saturate. At the same time the Schottky depletion layer and the heterojunction depletion layer are increasingly decoupled from each other.

From figure 9 it can be seen that the channel is completely depleted under the gate. As a result of equation (4), the electron density at the GaAs side is approximately proportional to the electron density at the AlGaAs side, since the normal current density is approximately zero under the gate.

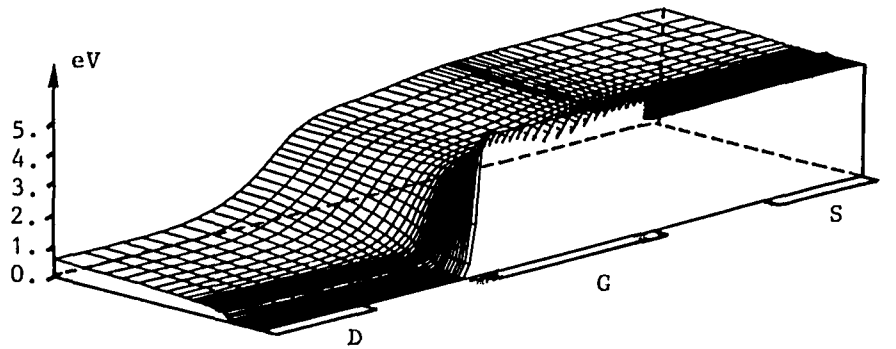

Fig.7 : Conduction band profile, V_{DS}=4.V, V_{GS}=0.V

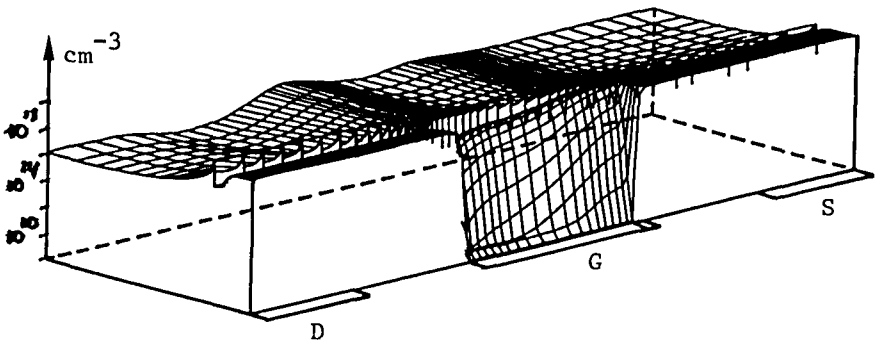

Fig.8 : Electron density, V_{DS}=4.V, V_{GS}=0.V

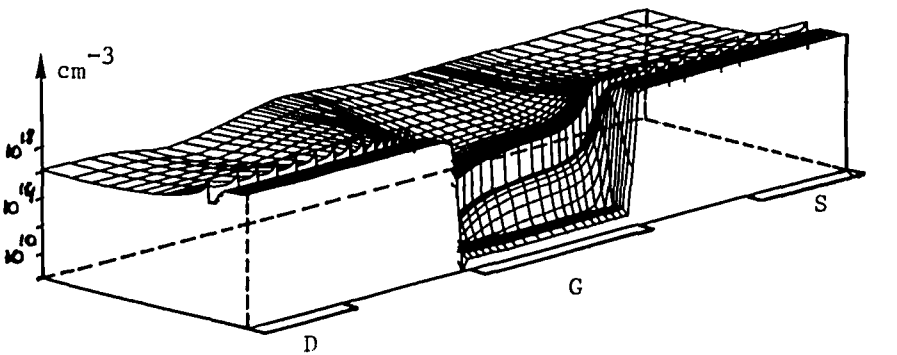

Fig.9 : Electron density, V_{DS}=4.V, V_{GS}=-1.8V

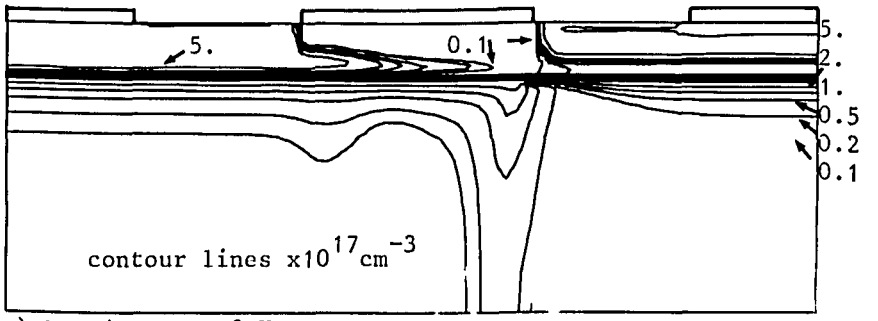

a) V_{DS}=4.V, V_{GS}=0.V

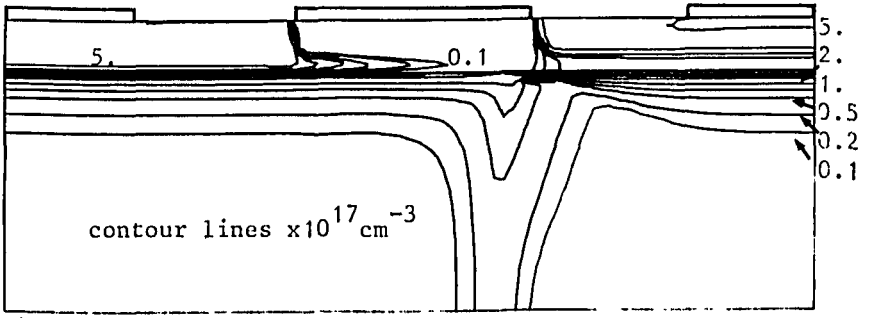

b) V_{DS}=4.V, V_{GS}=-0.6V

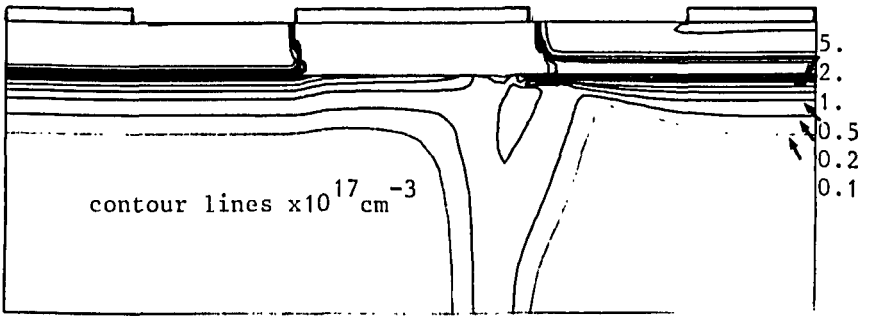

c) V_{DS}=4.V, V_{GS}=-1.2V

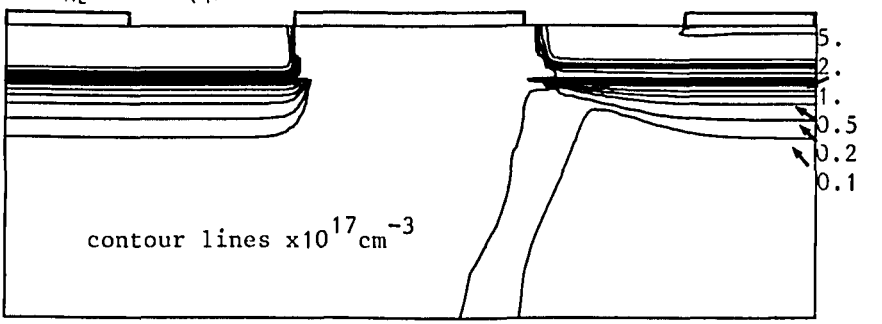

d) V_{DS}=4.V, V_{GS}= 1.8V

Fig.10 :Electron density drift-diffusion model

Tunneling turned out to be the most important conduction mechanism over the reverse biased heterojunction at the drain side. But with our choice of transport parameters (velocity-field relationship in the AlGaAs and barrier velocity $S_n = 10^7$ cm/s), its influence on external characteristics is rather low in both the on and off state, the current normal to the junction being limited by drift-diffusion in the heterojunction depletion layer.

Figure 11 shows the electron temperature distribution, as a result of the energy transport model simulations, for V_{DS} = 4.V and V_{GS} = -0.6V. At the drain end side of the channel, electrons gain energy from the high electric field. The electron temperature reaches a maximum of 10.000 K, which corresponds to an electron energy of 0.77 eV. A high electron temperature is also found in the AlGaAs layer at the drain side of the gate, which results in an electron density in this area higher than predicted from the drift-diffusion model (figure 12). This effect is enhanced by the fact that electrons from the channel can easily cross the heterojunction as they get an energy higher than the conduction band discontinuity, which was not predicted by the drift-diffusion model.

Figure 12 shows the electron density for V_{GS} = -0.6V and V_{DS} = 4.V. As the total amount of electrons in the AlGaAs layer has increased compared to the drift-diffusion model result presented in figure 10b, the current in the toplayer increases as well. However the contribution to the total current is still lower than 1%. In the part of the channel where electron temperature remains low, the total amount of electrons is the same for both models.

In the energy transport model, the current overthe reverse biased heterojunction at the drain side is established by hot electrons, having enough energy to cross the barrier without tunneling. This is not described by the drift-diffusion model.

Figure 13 shows a comparison of electron drift velocity in the channel, calculated with both models. The electron velocity predicted by the energy transport model is higher than the saturation velocity. This velocity overshoot effect results in a lower channel resistance, or equivalently in a 30% higher drain current.

5. CONCLUSION

A 2D drift-diffusion model and energy transport model have been used to simulate HEMT's and to illustrate device physics. For submicron HEMT's, hot electron effects such as velocity overshoot become important, so that the energy transport model should be considered to provide a more accurate description and a better understanding of the important phenomena. A comparison has been made with experimental results. Although the agreement is quite adequate, a more accurate knowledge of device and material parameters, especially drift-velocity data, is required to obtain a better fit.

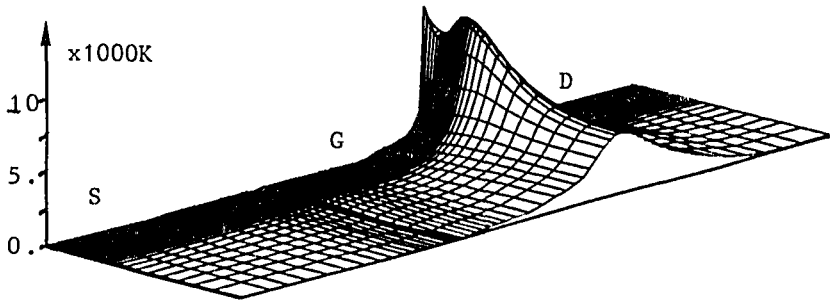

Fig.11 : Electron temperature distribution
V_{DS}=4.V, V_{GS}=-0.6V

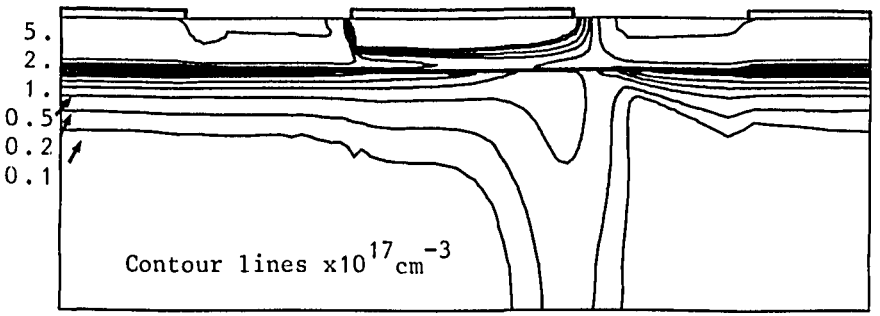

Fig.12 : Electron density from energy transport model.
V_{DS}=4.V, V_{GS}=-0.6V.

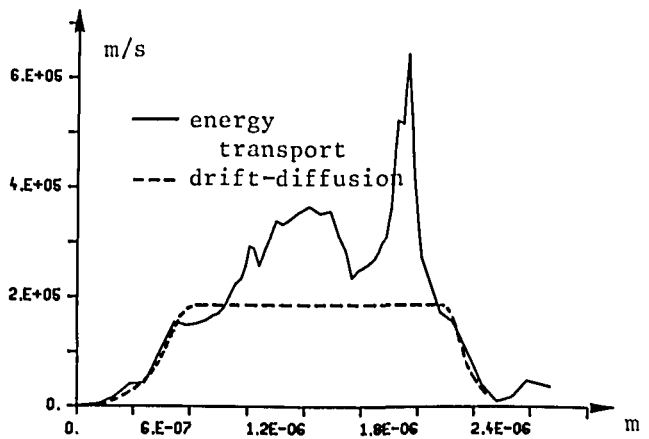

Fig.13 : Drift velocity in channel

REFERENCES

[1] DELAGEBEAUDEUF, D. and LIHN, N.T.,
"Metal-(n)AlGaAs-GaAs Two-Dimensional Electron Gas FET", IEEE Trans. Electron Devices, vol. ED-29, N°.6, pp. 955-960, June 1982.

[2] DRUMMOND, T.J., MORKOC, H., LEE, K. and SHUR, M.,
"Model for Modulation Doped Field effect Transistor", IEEE Electron Device Letters, vol. EDL-3, N°.11, pp. 338-341, November 1982.

[3] LEE, K., SHUR, M.S., DRUMMOND, T. and MORKOC, H.,
"Current-Voltage and Capacitance-Voltage Characteristics of Modulation-Doped Field-Effect Transistors", IEEE Trans. Electron Devices, vol. ED-30, N°.3, pp. 207-212, March 1983.

[4] LEE, K., SHUR, M.S., DRUMMOND, T. and MORKOC, H.,
"Parasitic MESFET in (Al,Ga)As/GaAs Modulation Doped FET's and MODFET Characterisation", IEEE Trans. Electron Devices, vol. ED-31, N°.1, pp. 29-35, January 1984.

[5] REISER, M.,
"A Two-Dimensional Numerical FET Model for DC, AC, and Large-Signal Analysis", IEEE Trans. Electron Devices, vol. ED-20, N°.1, pp. 35-45, January 1973.

[6] SELBERHERR, S.,
"Analysis and Simulation of Semiconductor Devices", Springer-Verlag, Wien, New York

[7] SNOWDEN, C.M., HOWES, M.J. and MORGAN, D.V.,
"Large Signal Modelling of GaAs MESFET Operation", IEEE Trans. Electron Devices, vol. ED-30, N°.12, pp. 1817-1824, December 1983.

[8] CURTICE, W.R. and YUN Y.H.,
"A Temperature Model for the GaAs MESFET", IEEE Trans. Electron Devices, vol. ED-28, N°.8, pp. 954-962, August 1981.

[9] COOK, R.K. and FREY, J.,
"Two-Dimensional Numerical Simulation of Energy Transport Effects in Si and GaAs MESFET's", IEEE Trans. Electron Devices, vol. ED-29, N°.6, pp. 970-977, June 1982.

[10] SNOWDEN, C.M.,
"Numerical Simulation of Microwave GaAs MESFET's", In: Proceedings of International Conference on Simulation of Semiconductor Devices and Processes, Pineridge Press, Swansea, July 1984.

[11]YOSHIDA, J. and M. KURATA, M.,
"Analysis of High Electron Mobility Transistors Based on a Two-Dimensional Numerical Model"; IEEE Electron Device Letters, vol. EDL-5, N°.12, pp. 508-510, December 1984.

[12]TANG, J.Y.F.,
"Twodimensional Simulation of MODFET and GaAs Gate Heterojunction FET's", IEEE Trans. Electron Devices, vol. ED-32, N°.9, pp. 1817-1823, September 1985.

[13]WIDIGER, D., Hess, K. and Coleman, J.J,
"Twodimensional Numerical Analysis of the High Electron Mobility Transistor", IEEE Electron Device Letters, vol. EDL-5, N°.7, pp. 266-269, July 1984.

[14]WIDIGER, D., KIZILYALLI, I.C., HESS, K. and COLEMAN, J.J.,
"Two-Dimensional Transient Simulation of an Idealized High Electron Mobility Transistor", IEEE Trans. Electron Devices, vol. ED-32, N°.6, pp. 1092-1102, June 1985.

[15]BENNETT, H.S.,
"Modeling GaAs/AlGaAs Devices: A Critical Review"; IEEE Circuits and Devices Magazine, January 1985, pp. 35-42.

[16]CASEY, H.C and PANISH, M.B.,
"Heterostructure Lasers. Part A: Fundamental Principles", Academic Press, New York, 1978.

[17]SCHUELKE, R.J. and LUNDSTROM, M.S.,
"Thermionic Emission-Diffusion Theory of Isotype Heterojunctions", Solid State Electronics, vol. 27, N°.12, pp. 1111-1116, 1984.

[18]GRINBERG, A.A., SHUR, M.S., FISHER, R.J. and MORKOC, H.,
"An Investigation of the Effect of Graded Layers and Tunneling on the Performance of AlGaAs/GaAs Heterojunction Bipolar Transistors", IEEE Trans. Electron Devices, vol. ED-31, N°.12, pp. 1758-1765, December 1984.

[19]YOSHIDA, J.,
"Classical versus Quantummechanical Calculation of the Electron Distribution at the n-AlGaAs/GaAs Hererointerface", IEEE Trans. Electron Devices, vol. ED-33, N°.1, pp. 154-156, January 1986.

[20]TANG, T.W.,
"Extension of the Scharfetter-Gummel Algoritm to the Energy Balance Equation", IEEE Trans. Electron Devices, vol. ED-31, N°.12, pp. 1912-1914, December 1984.